Published in final edited form as:
Nanomedicine (Lond). 2013 June ; 8(6): 875–890. doi:10.2217/nnm.12.137.

Near-infrared fluorescent imaging of metastatic ovarian cancer using folate receptor-targeted high-density lipoprotein nanocarriers

Ian R Corbin[*,1], **Kenneth K Ng**[2], **Lili Ding**[3], **Andrea Jurisicova**[4], and **Gang Zheng**[2,3]

[1]Advanced Imaging Research Center, University of Texas Southwestern Medical Center at Dallas, Dallas, TX 75390, USA

[2]Institute of Biomaterials & Biomedical Engineering, University of Toronto, ON M5G 1L7, Canada

[3]Department of Medical Biophysics, University of Toronto, Ontario Cancer Institute, Toronto, ON M5G 1L7, Canada

[4]Department of Obstetrics & Gynecology, Samuel Lunenfeld Research Institute, Mount Sinai Hospital, University of Toronto, ON M5G 1X5, Canada

Abstract

Aim—The targeting efficiency of folate receptor-α (FR-α)-targeted high-density lipoprotein nanoparticles (HDL NPs) was evaluated in a syngeneic mouse model of ovarian cancer.

Materials & methods—Folic acid was conjugated to the surface of fluorescent-labeled HDL NPs. *In vivo* tumor targeting of folic acid-HDL NPs and HDL NPs were evaluated in mice with metastatic ovarian cancer following intravenous or intraperitoneal (ip.) administration.

Results & discussion—Intravenous FR-α-targeted HDL resulted in high uptake of the fluorescent nanoparticle in host liver and spleen. The ip. injection of fluorescent HDL produced moderate fluorescence throughout the abdomen. Conversely, animals receiving the ip. FR-α-targeted HDL showed a high fluorescence signal in ovarian tumors, surpassing that seen in all of the host tissues.

Conclusion—The authors' findings demonstrate that the combination of local–regional ip. administration and FR-α-directed nanoparticles provides an enhanced approach to selectively targeting ovarian cancer cells for drug treatment.

Keywords

folate receptor; lipoprotein; local-regional treatment; nanoparticle; near-infrared fluorescence imaging; ovarian cancer

Ovarian cancer is a major cause of morbidity and mortality among women with gynecological malignancies worldwide [1]. In the USA alone each year over 21,000 women will be diagnosed with ovarian cancer, and sadly within this same time period more than 15,000 women will succumb to this disease [2]. These grim statistics arise from the fact that

[*]Author for correspondence: Tel.: +1 214 645 7044 Fax: +1 214 645 2744 ian.corbin@utsouthwestern.edu.

Financial & competing interests disclosure The authors have no other relevant affiliations or financial involvement with any organization or entity with a financial interest in or financial conflict with the subject matter or materials discussed in the manuscript apart from those disclosed.

ovarian cancer typically follows a clinically silent course that is largely asymptomatic in the early stages; therefore at the time of diagnosis patients often present with advanced metastatic spread beyond the ovaries (stage III or IV). At this advanced stage, the prognosis is poor for this disease, and the 5-year survival rates for stage III and IV patients with ovarian cancers are typically as low as 43 and 17%, respectively [3]. Although metastatic disease in ovarian cancer is usually confined to the abdominal (peritoneal) cavity, improvements in the treatment of this cancer have been gradual [4,5]. The best response rates are achieved through a combination of debulking surgery (to remove main tumor mass) followed by an aggressive course of adjuvant chemotherapy (platinum–taxane combination regime) [6]. Intraperitoneal (ip.) administration of chemotherapy offers an appealing approach to treating metastatic ovarian cancer. Indeed, several clinical trials have demonstrated a survival advantage among advanced ovarian cancer patients following treatment with localized ip. chemotherapy [7,8]. Despite this therapeutic advantage, many patients undergoing ip. chemotherapy, like intravenous (iv.) therapy, suffer from systemic toxicities [9–11]. In fact, grade 3 and 4 toxicities have been reported following treatment with ip. chemotherapy. Moreover, such side effects are commonly reported as the reason for treatment discontinuation [12,13]. Clearly, if the benefits of ip. local–regional therapy are to be fully exploited in this disease, cancer targeting/host tissue-sparing strategies should be employed.

To date, a number of molecular targets for ovarian cancer are currently being explored to avoid the collateral tissue damage associated with indiscriminate therapies. The folate receptor-α (FR-α) has been recognized for some time as a marker of malignant transformation in the ovary [14,15]. Over 90% of nonmucinous ovarian cancers overexpress FR-α and the degree of FR-α expression correlates with the grade of malignancy [14]. This cell surface glycoprotein receptor provides a high-affinity route for the internalization of the vitamin folic acid (FA), which confers a growth advantage to these malignant cells [16]. The FR-α is an attractive candidate for targeted therapy because, unlike the ubiquitously expressed reduced folate carrier, the FR-α has a limited expression pattern in normal tissues (mainly apical surface of placenta, choroid plexus and kidney tubules) [15]. Moreover the FR-α is a robust transporter, allowing the internalization of FA conjugates of low-molecular-weight compounds, proteins or nanoparticles (NPs) [17,18]. Indeed, numerous preclinical [19–21] and clinical [22–24] studies have validated the *in vivo* targeting of FA conjugates for cancer.

Previous studies have shown that engineered high-density lipoprotein (HDL) NPs are a versatile and effective drug-delivery platform [25]. They share similar nanoscale dimensions, pharmacokinetics and receptor-binding properties as their endogenous counterparts. Furthermore, HDL NPs are fully biocompatible, nonimmunogenic and naturally able to mitigate the reticular endothelium system (RES). Although the HDL NP offers many incentives as a delivery vehicle, HDL receptor (scavenger receptor class B type I [SR-BI]) targeting offers little specificity for cancer-directed strategies. Enhanced tumor targeting of this carrier can be achieved by attaching cancer-homing molecules to the apoAI component of the HDL NP [26,27]. Corbin *et al.* demonstrated this by conjugating FA molecules to the apoprotein component of HDL NPs [27]. Following FA conjugation, HDL NPs no longer possess binding avidity to the SR-BI, instead the particle is actively rerouted to the FR-α. Both *in vitro* and *in vivo* experiments have demonstrated that the FA-conjugated HDL (FA-HDL) can avidly bind and be internalized in FR-α-expressing cancer cells [27].

The present study evaluates the utility of FA-HDL NPs in a murine model of metastatic ovarian cancer. The combined strategy of using FR-α-directed NPs and local–regional ip.

administration is assessed for its capacity to provide enhanced targeting to ovarian cancer cells.

Materials & methods

Preparation of near-infrared fluorescent dye: DiR-BOA

1,1'-dioctadecyl-3,3,3',3'-tetramethylindo-tricarbocyanine iodide bis-oleate (DiR-BOA) was synthesized according to the methods previously described [27].

Preparation of apoAI

HDL was isolated from fresh plasma of healthy donors by sequential ultracentrifugation [28]. The HDL fraction was subsequently subjected to standard ethanol:diethylether 3:2 (v/v) delipidation [29] to extract apo-HDL proteins, mainly apoAI. The final apoAI preparations were resuspended in 4 M urea and stored at −20°C until HDL NPs were prepared.

Formulation of FA-HDL(DiR-BOA) NPs

Reconstituted HDL(DiR-BOA) NPs were prepared by the cosonication method similar to that described by Pittman *et al.* [30]. ApoAI, egg yolk phosphatidyl choline, cholestryl oleate and DiR-BOA were formulated at a molar ratio of 1:22:5:14, respectively. First, a film of the lipids and DiR-BOA, dried under nitrogen, was resuspended in warm (50°C) sonication buffer (10 mM Tris-HCl, pH 8.0, containing 0.1 M KCl, 1 mM EDTA) with intermittent vortexing. Following vortexing, the mixture was sonicated for 60 min at 49–54°C under nitrogen. After the first sonication step, the emulsion mixture was filtered (0.1-μm filter) to remove large emulsion complexes. The temperature of the sonication bath was then lowered to 40–42°C and sonication was continued. During this period, apoAI in 4 M urea was added in small portions to the emulsion mixture over 10 min and sonication was continued for an additional 20 min. The heterogenous mixture of HDL(DiR-BOA) particles was then filtered (0.1 μm). The HDL(DiR-BOA) particles were then purified by gel filtration chromatography using a Superdex™ 200 column (60 × 16 cm) with the Akta™ FPLC system (Amersham Biosciences, PA, USA). Appropriate fractions were collected and stored at 4°C until FA conjugation. Just prior to folate conjugation, the solution of HDL(DiRBOA) was adjusted to a pH of 10.7 with sodium phosphate/boric acid buffer (0.1 M NaH_2PO_4, 0.1 M H_3BO_3 and 1 mM EDTA). The folate conjugated reaction was performed similar to that described for FA–low-density lipoprotein (LDL) conjugates [31].

In vitro NP characterization

Composition

The molar concentration of apoAI was determined using a commercial Lowry protein assay kit (Sigma-Aldrich, MO, USA) using a molecular weight of 28,000 Da. DiR-BOA content was determined by organic chloroform:methanol (2:1) extractions. Following complete extraction, the organic layer was removed and dried, the DiR-BOA residue was brought up in a fixed volume of chloroform and its fluorescence intensity read using a spectrofluorometer (excitation 748 nm; emission 780 nm). The concentration of DiR-BOA in the sample was calculated based on a standard curve of DiR-BOA. The number of FA molecules attached to HDL NPs was determined from the unique UV absorbance of FA at 280 nm, as described previously [31]. Finally, to determine the composition of these components per particle, we calculated their molar ratios relative to apoAI and we assumed that each HDL NP contained two to three molecules of apoAI proteins [32].

Dynamic light scattering

The particle size distributions (volume mode) of HDL NPs were measured by light-scattering photon correlation spectroscopy (Zetasizer Nano-ZS90; Malvern Instruments, Worcestershire, UK) utilizing a 4.0-mW He–Ne laser operating at 633 nm and a detector angle of 90°. The data were modeled assuming spherical particles undergoing Brownian motion.

Circular dichroism spectroscopy

Far-UV circular dichroism (CD) spectra of HDL NPs were recorded using a Jasco J-815 CD spectrometer (Jasco, Inc., MD, USA). The CD spectra were recorded at 25°C with a 1-nm step size from 260 to 190 nm. The data were collected over five consecutive scans and averaged. The a-helix secondary structure of apoAI was monitored by changes in ellipticity at 222 nm.

Agarose electrophoresis

The electrophoretic properties of HDL NPs were examined by 1.0% agarose gel electrophoresis. Samples (10 μg) were applied to gel wells and allowed to penetrate into gel for 5 min before the electric field was applied. Electrophoresis was performed at a voltage of 130 V for a duration of 30 min at 25°C in barbital buffer (pH 8.6; 0.05 ionic strength). After electrophoresis, the migration of the HDL NPs was visualized by Coomassie staining.

In vitro functional assays

Cell culture

LdlA(murine SR-BI [mSR-BI]) and ldlA7 were gifts from Monty Krieger (Massachusetts Institute of Technology, MA, USA). LdlA(mSR-BI) cells were cultured in F-12K medium (Ham's Nutrient Mixture) with 2 mM l-glutamine, 100 U/ml penicillin–streptomycin, 300 μg/ml active G418 and 5% fetal bovine serum. LdlA7 cells were cultured under similar conditions without G418. Transformed mouse ovarian surface epithelial cells (MOSECs), clonal line IC5, were generously obtained from Katherine Roby (University of Kansas Medical Center, Center for Reproductive Sciences, KS, USA). The IC5-MOSECs were cultured in DMEM supplemented with 4% fetal bovine serum, 100 U/ml penicillin–streptomycin, 5 μg/ml insulin, 5 μg/ml transferrin and 5 ng/ml sodium selenite. All cells were grown at 37°C in a humidified atmosphere containing 5% CO_2.

Confocal microscopy & flow cytometry

Laser scanning confocal microscopy studies were performed on an Olympus FV1000 laser confocal microscope (Olympus, Tokyo, Japan) operating at an excitation wavelength of 633 nm. Complimentary flow cytometry experiments were conducted on Beckman Coulter FC500 five color analyzer (Beckman Coulter, ON, Canada) similarly operating with an excitation wavelength of 633 nm. In brief, cells grown on eight-well Lab-Tek™ chamber slides (Nunc Lab-Tek, Sigma-Aldrich) for confocal microscopy or in a six-well cell culture dish for flow cytometry studies. The cells were treated with indicated amounts of HDL(DiR-BOA), FA-HDL(DiR-BOA) and/or excess unlabeled native HDL and/or excess FA. After 3 h incubation at 37°C, all cells were washed with phosphate-buffered saline (PBS), and those designated for confocal microscopy were overlaid with appropriate culture media and directly investigated by live cell imaging. For flow cytometry analysis, the cells were liberated from the wells with trypsin-EDTA (0.25%), washed several times in PBS and finally resuspended in FACS buffer.

Animals

Induction of metastatic ovarian cancer

The following protocol was approved by the Animal Care Committee at the University Health Network (ON, Canada). Retired adult female C57BL6 breeder mice were allowed free access to food and water throughout the study. IC5-MOSECs (5×10^6 each) were inoculated directly into the peritoneal cavity of each mouse. Approximately 3 months later, when the mice showed initial signs of ascites, the animals were used in the subsequent experiments.

Near-infrared fluorescence imaging

The mice were randomly allocated to either receive an ip. injection of FA-HDL(DiR-BOA) or HDL(DiR-BOA) or a tail vein iv. injection of FA-HDL(DiR-BOA) at a dose of 4 nmol DiRBOA per animal. After 24 h the animals were sacrificed and whole-body fluorescence imaging was performed. Fluorescent images were obtained with a CRI Maestro™ *in vivo* imaging system (CRI, MA, USA). To obtain images of the abdominal organs, the abdomen was opened and the ascites fluid collected. The animal was placed supine inside the imaging chamber of the Maestro scanner. Fluorescent images of the DiR-BOA fluorescence were acquired with a deep red filter set (excitation: 671–705 nm; emission: 750 nm long pass) with an exposure time of 500 ms. Following the whole-body imaging, various organs and the metastatic tumors were excised and also imaged.

Biodistribution

The excised organs (liver, spleen, heart, muscle, kidney, adrenals, ovaries and brain) and tumor tissue from mice were harvested, weighed and homogenized in PBS. Homogenates were then combined with a threefold excess of a chloroform:methanol (2:1) mixture, and vortexed for 3 min. Solutions were subsequently centrifuged at 10,000 rpm for 10 min. The fluorescence intensities of the various samples were measured (excitation: 748 nm; emission: 785 nm) using a Fluoromax®-4 spectrofluorometer (Edison, NJ, USA). Tissue fluorescence of the extract was measured and presented as fluorescent intensity per unit (mg) tissue. For analysis of the ascites collection, the samples were centrifuged (2000 rpm for 5 min) to separate the cell and supernatant components. The cell fraction was subsequently washed twice with PBS and treated with red blood cell lysis buffer (0.1% potassium bicarbonate, 0.8% ammonium chloride, 0.1 mM EDTA) for 10 min to remove the red blood cells. Cells were counted with a hemocytometer using an inverted microscope, and then extracted with chloroform:methanol (2:1). DiR-BOA fluorescence of the cell extract was measured and presented as fluorescent intensity per million cells. An aliquot of the ascites supernatant fraction was also extracted with chloroform:methanol (2:1) and analyzed on the fluorometer to determine the amount of free-floating HDL NPs in the ascites fluid.

Results

The cosonication method produced a heterogenous mixture of fluorescent HDL NPs of various sizes (Supplementary Figure 1a, see online at www.futuremedicine.com/doi/suppl/10.2217/ nnm.12.137). Following gel filtration chromatography, three distinct populations were identified. Particles eluting in the sharp peak at 46 min were large particles (hydrodynamic diameter >20 nm) that pass in the void volume. The broad peak at 62 min contained most of the HDL NP core loaded with DiR-BOA, which can be seen by the deep green coloration of these fractions (Supplementary Figure 1a). Calibration of the FPLC Superdex 200 column indicates that the peaks eluting at a retention time of 62 min correspond to particles with a diameter of approximately 11 nm. Dynamic light scattering was later performed and it was determined that the HDL(DiR-BOA) NPs from these

fractions possess a slightly larger diameter of 15.8 ± 3.2 nm (Supplementary Figure 1B). The last population of particles eluting at 75 min were much smaller structures with little DiR-BOA content. The HDL(DiR-BOA) NPs collected at 62 min were used for all subsequent experiments. The compositional analyses of these particles revealed that each HDL NP contained four molecules of DiR-BOA dye.

Functional analyses, which involved testing HDL(DiR-BOA) NP affinity for the HDL receptor (SR-BI), were performed in cell culture experiments with cells that overexpressed SR-BI (LdlA[mSR-BI]) and cells lacking SR-BI expression (ldlA7). Following a 3-h incubation, LdlA(mSR-BI) displayed strong fluorescence uniformly throughout the cell cytoplasm (Supplementary Figure 2). Conversely, ldlA7 showed only trace amounts of fluorescence after the 3-h incubation period. Quantitative flow cytometry indicated that the fluorescence in LdlA(mSR-BI) was nearly six-times greater than that in ldlA7 cells (Supplementary Figure 3). These findings reflect the high expression of SR-BI and the corresponding high uptake of HDL(DiR-BOA) in LdlA(mSR-BI) cells relative to that in ldlA7 cells. Furthermore, when HDL NPs were coincubated with excess native HDL, HDL(DiR-BOA) uptake in LdlA(mSR-BI) was significantly inhibited. These findings further confirm that the uptake mechanisms of HDL NPs are SR-BI mediated. As expected, excess native HDL had little to no effect on the uptake of HDL(DiR-BOA) in ldlA7 cells.

FA conjugation of HDL(DiR-BOA) yielded particles that contained four molecules of DiR-BOA dye and 44 molecules of FA (Figure 1a). Scanning UV spectrometry displayed both of these features of the NP (Figure 1B). CD spectrometry was also performed to document the protein secondary structure of the apoAI component in the HDL NPs (Figure 1C). While apoAI in native HDL had a higher content of α-helix than that found in the manufactured HDL NPs, FA-HDL(DiR-BOA) and HDL (DiR-BOA) had similar levels of α-helix in their apoAI protein. In addition, agarose gel electrophoresis revealed that FA-HDL(DiR-BOA) possesses an increased electrophoretic mobility compared with native HDL (data not shown). Finally, dynamic light scattering experiments showed that the FA-HDL(DiR-BOA) NP possessed an average diameter of 14.17 ± 3.29 nm.

Confocal and flow cytometry experiments were performed to assess the FR-α targeting of FA-HDL (DiR-BOA) in the IC5-MOSEC line (Figures 2 & 3). In these experiments, IC5-MOSECs were incubated with HDL(DiR-BOA) or FA-HDL(DiR-BOA). Following a 3-h incubation period, negligible amounts of HDL(DiR-BOA) were taken up in IC5-MOSECs. Conversely, under the same conditions, high amounts of FA-HDL(DiR-BOA) were actively internalized in these cells. Clearly, the FA moieties facilitated the uptake of the HDL NPs into the IC5-MOSECs; additional experiments were performed to assess the importance of the FR in this process. Competition experiments were then performed by incubating IC5-MOSECs with FA-HDL(DiRBOA) and excess HDL or FA or a combination of both. Excess native HDL failed to have any effect on the uptake of FA-HDL(DiR-BOA). Conversely, free FA significantly lowered the uptake of FA-HDL(DiR-BOA) into the cells and the combination of excess HDL and free FA did not further potentiate the inhibition seen by free FA alone. Collectively, these findings indicate that FR rather than SR-BI is the primary receptor responsible for the uptake of FA-HDL(DiRBOA) in IC5-MOSECs. Previous studies by the authors have shown that by conjugating FA moieties to the apoAI component of the HDL, one effectively abolishes the HDL NP affinity for SR-BI and actively reroutes it to the FR-α [27]. Given that IC5 cells seemingly have much higher FR-α expression than SR-BI, this strategy significantly enhances the drug-delivery capacity of the HDL NP to these cells.

Supplementary confocal experiments were also performed to demonstrate the differences between SR-BI- and FR-α-mediated uptake processes (Supplementary Figure 4). When

HDL(DiR-BOA) interact with ldlA(SR-BI) cells it is the SR-BI receptor that primarily mediates the internalization of DiR-BOA into the cell. This process gives rise to a strong diffuse fluorescence pattern that shows little overlap with the endocytic marker, lysotracker. When IC5-MOSECs are incubated with HDL(DiR-BOA) under similar conditions, a sparse punctuate fluorescent pattern is seen with moderate amounts of coregistration with lysotracker. Finally, the uptake of FA-HDL(DiR-BOA) into IC5-MOSECs produces pronounced punctuate fluorescence throughout the cell with significant overlap with lysotracker. These results clearly show that the intracellular fluorescence pattern generated by FR-α uptake is distinctly different from that produced by SR-BI mediated uptake.

A syngeneic mouse model of metastatic ovarian cancer was produced by injecting 5 million IC5-MOSECs into the peritoneal cavity of mature C57BL6 female mice. A total of 3 months following the tumor cell inoculation, hemorrhagic ascites develop that distend the abdomen of these animals (Figure 4A). The ascites, which could be as much as 10 ml at this stage, consisted mainly of tumor cells and host immune cells and red blood cells. Also present at this time are small (≤1 cm) metastatic tumors throughout the peritoneal cavity of the mouse that cover the omentum, viscera, diaphragm and peritoneal walls (Figures 4B & 4C). Actual invasion of the tumors into the abdominal organs was not seen, nor was there any evidence of tumors outside the peritoneal cavity.

Once at this stage, mice were allocated to one of three groups, where they received either an iv. injection of FA-HDL(DiR-BOA), an ip. injection of HDL(DiR-BOA) or an ip. injection of FA-HDL(DiR-BOA). A total of 24 h following the administration of the HDL NPs, the animals were euthanized and their abdomen exposed for fluorescent imaging. Distinctly different fluorescence distribution patterns were seen between the different treatment groups (Figures 5A–5C). Animals that received iv. FA-HDL(DiR-BOA) displayed intense fluorescence signal localized primarily to the liver. Little fluorescence could be detected outside the liver (Figure 5A). Ip. injection of HDL(DiR-BOA) resulted in moderate amounts of fluorescence in the liver and throughout the abdomen (Figure 5B). Finally, for mice that were injected ip. with FA-HDL(DiR-BOA), a grainy diffuse pattern of fluorescence was seen across the abdomen and little to no fluorescence was observed in the liver (Figure 5C).

Following whole-body fluorescence imaging, various organs and tumor foci were excised and imaged in a 12-well plate to get a clearer view of the biodistribution of the HDL NPs (Figures 6A–6C). *Ex vivo* images of the tissues from the iv. FA-HDL(DiR-BOA) group were consistent with the whole-body images, practically all of the injected dose of the FA-HDL NPs was taken up by the liver (Figure 6A). The ip. HDL(DiR-BOA) group also had strong fluorescence in the liver, but moderate amounts of fluorescence could also be seen in the kidneys, adrenals, ovaries and tumors (Figure 6B). *Ex vivo* images from the ip. FA-HDL(DiR-BOA) treatment group revealed strong fluorescence in the diaphragmatic tumor foci, medium fluorescence in the remaining abdominal tumors and little to no fluorescence was seen in any of the host's tissues (Figure 6C).

Finally, fluorescence readings from the organic extracts of the tissue samples were performed to get a more quantitative measure of the biodistribution (Figure 7). Iv. injection of FA-HDL NPs had the highest intensity of fluorescence in the liver; on the other hand, ip. injection of FA-HDL NPs had the highest levels of fluorescence in the tumor. Finally, ip. injection of HDL(DiR-BOA) had moderate amounts of fluorescence across the mouse tissues and tumors. Similar quantitative analysis was also performed on the ascites collection (Figures 8 & 9), and animals treated with FA-HDL(DiR-BOA) ip. displayed the greatest fluorescence in the cellular compartment (nearly 400- and seven-times greater than that in the iv. FA-HDL[DiR-BOA] and ip. HDL[DiR-BOA] groups, respectively) (Figure 8). This group also had the least fluorescence in the ascites cell free-fluid fraction (Figure 9).

Conversely, HDL(DiR-BOA) ip. had greater fluorescence in the cell free-fluid fraction compared with the cellular compartment. Little to no fluorescence was detected in the cell or fluid compartments of the ascites from mice given iv. FA-HDL(DiR-BOA).

Discussion

Within recent years, lipoprotein-based NPs have increasingly been identified as viable and attractive drug-delivery systems [33–38]. The nonpolar core compartment of the lipoprotein NP has been shown to be a suitable depot for hydrophobic drugs and imaging agents [39,40]. Meanwhile, the protein–phospholipid shell of this nanostructure presents as an autogenous surface to its biological environment, which neither elicits an immunogenic nor a RES response. The interweaving surface apoproteins of the lipoprotein provide fine size control of these particles through a complex network of amphipathic α-helix and/or β-sheet proteins. Furthermore, the apoprotein component of lipoprotein imparts the receptor recognition or targeting functionality for selective receptor-mediated uptake of the particle [41,42]. The overexpression of lipoprotein receptors on various cancer cells has made the lipoprotein system an attractive targeting approach for cancer therapy and imaging. Indeed, numerous studies have been performed where HDL or LDL receptors were targeted for NP-directed treatment or detection of tumors [39,43,44]. While SR-BI and the LDL receptors provide selective uptake of HDL and LDL NPs, respectively, these receptors are not specific for cancer cells. In fact, the high expression of these receptors in the liver, reproductive tissues and adrenal glands often compromises the efficacy of lipoprotein-mediated drug delivery. It was for these reasons that the lipoprotein rerouting strategy was employed [31]. By covalently conjugating cancer-specific small-molecule ligands to the lysine residues of the apoprotein, one effectively eliminates the lipoprotein's affinity for its native receptor and redirects the lipoprotein NP towards the ligand designated (cancer specific) surface epitope/receptor [26,31]. This strategy was successfully demonstrated by rerouting LDL and HDL NPs to the FR-α by attaching FA to their apoproteins [27,31,45]. The FR-α has long been considered an optimal target for cancer therapy due to its high affinity for FA conjugates [17,18], overexpression in malignant cells and restricted expression in normal tissues [46]. The FR-α is a particularly attractive biomarker for ovarian cancer as it is consistently overexpressed in the majority of nonmucinous epithelial tumors [47], and it has been shown to have a discrete role in the biology of this cancer [14].

In the present study, the malignant murine ovarian cell line IC5-MOSEC, like its human counterpart, was also shown to express high levels of FR-α. The advantage of FR-α targeting in IC5-MOSECs was clearly demonstrated in our studies. Initial targeting experiments were performed with the HDL NP alone; precedence for this approach stemmed from previous publications that promoted SR-BI-directed drug delivery for ovarian cancer [33]. Surprisingly, in the present study, HDL NPs were shown to have little interaction with IC5-MOSECs, and western blot analysis later confirmed these findings, showing that these cells displayed weak expression for SR-BI protein. Subsequently, when FA was conjugated to the HDL NP, its targeting efficiency was markedly improved. Additional inhibition experiments with excess free FA verified that the enhanced uptake of the FA-HDL NP was indeed mediated by the FR-α. Evidence for synergistic contributions from residual SR-BI binding proved to be negligible as excess HDL did not impede upon the uptake of FA-HDL(DiR-BOA) in IC5-MOSECs. A pronounced punctuate pattern of fluorescence could be seen throughout these cells following incubation with FA-HDL(DiR-BOA). Coregistration of the DiR-BOA fluorescence with that of lysotracker confirms that the FA-HDL NP was internalized through an endocytic pathway and later deposited into lysosomes. This mechanism of uptake is distinctly different from that of SR-BI (selective lipid transfer) [48]. Only partial coregistration of DiR-BOA and lysotracker were evident in IC5-MOSECs following HDL(DiR-BOA) treatment, which suggests that some nonspecific whole-particle

uptake processes together with SR-BI selective lipid transport was responsible for this particle's binding and uptake. By contrast, HDL(DiR-BOA) incubation with LdlA(mSR-BI) (mutant Chinese ovarian hamster cells that overexpress SR-BI) [49] produces a diffuse intracellular fluorescence pattern with little to no overlap with lysotracker, indicative of predominate SR-BI-mediated uptake. Overall, the findings of these cell studies validate the lipoprotein rerouting strategy and moreover emphasize the importance FR-α targeting for the intracellular delivery of NPs in ovarian cancer cells. A recent paper by Werner *et al.* supports this premise, as promising therapeutic results were achieved using a folate-targeted poly($_{D,L}$-lactide-*co*-glycolide) (PLGA) polymer NP system against human ovarian cancer cells [50].

The introduction of IC5-MOSECs into the ovarian bursa or peritoneal cavity of syngeneic female mice (C57BL6 background) produces metastatic ovarian cancer similar to that seen in humans [51]. Tumor foci develop and spread throughout the abdominal cavity, and in the advanced stage of this disease a pronounced hemorrhagic ascites also develops. Although this malignancy is confined to the peritoneal cavity, efficient targeting to these cancer cells still remains a challenging task during clinical and preclinical therapy. Direct ip. delivery of antineoplastic agents would appear to be a rational approach to treat this cancer; however, patients can still succumb to significant toxicities that compromise therapy [52,53]. Regional administration of conventional low-molecular-weight cytotoxic drugs (<20 kDa) are problematic as they are indiscriminant (taken up by malignant and normal tissues) and are rapidly absorbed through the peritoneal capillaries allowing them entry into the systemic circulation (thus minimizing the advantages of local delivery) [54]. These compromises probably explain the reports of adverse toxicity and limited efficacy associated with ip. chemotherapy. Use of a colloid NP, such as the FA-HDL NP, should provide a number of benefits for local–regional drug delivery. In this section of our study, the tumor-targeting efficacies of the HDL-based NPs were examined following iv. (systemic) and ip. (local–regional) administration. The importance of regional NP administration and active targeting are highlighted.

Systemic administration of NPs has been the traditional approach for most researchers to deliver diagnostic/therapeutic agents to solid tumors. The tortuous and leaky vasculature of growing tumors provides the `enhanced permeability and retention' effects to retain NPs in the tumor vicinity, allowing for nonspecific uptake or binding to occur. Alternatively, if active targeting strategies are employed, the NP can specifically bind to and be internalized by the cancer cells. These events, however, can only occur if the NP is able to first escape RES surveillance and avoid specific (active targeting) or nonspecific uptake by normal cells. These barriers probably explain why typical antibodies and NPs have such poor tumor-targeting efficacies (0.001–000.01% and 2–8% of initial injected dose, respectively) [55–57]. Poor tumor targeting was also seen when FA-HDL(DiR-BOA) was systemically administered to mice with metastatic ovarian cancer. Very few NPs actually made it into the peritoneal cavity to be taken up by the IC5-MOSECs, instead the majority of the NPs were retained by the liver. Biodistribution analyses showed that the fluorescence signal within the liver greatly exceeded that from the IC5-MOSEC tumors by 150- to ≥200-times. Traditional pharmacological modeling indicates that the peritoneal cavity is a distinct and separate compartment from the systemic vasculature. In this model, the FA-HDL NPs seem to more easily transition from the systemic vasculature into the hepatic interstitial space than into the peritoneal cavity. Furthermore, the high expression of the reduced folate carrier and proton-coupled folate transporters in the liver [58–60] probably explains the high hepatic uptake of FA-HDL(DiR-BOA). Although these carriers are not high-affinity systems for FA uptake [58], the high blood flow through the liver combined with the high hepatic expression of these transporters enables this system to effectively sequester most of the iv. FA-HDL NPs.

Ip. administration of the HDL-based NPs was then performed to overcome the compartmental barriers associated with iv. delivery. Studies by Yeo and Xu, however, point out that local–regional delivery of NPs does not guarantee efficacious tumor targeting [61]. This was seen as the ip. injection of HDL(DiR-BOA) into tumor-bearing mice failed to show significant uptake of these particles into the IC5-MOSEC tumors or in the ascites metastatic cells. Subsequent analyses of the mice ascites fluid revealed that the majority of HDL NPs remained in the cell-free fraction of the ascites. As was illustrated earlier, IC5-MOSECs express low levels of SR-BI, thus any uptake of HDL NPs that does occur in these cells primarily proceeds through nonspecific interactions. These passive uptake processes were simply incapable of mediating high uptake of HDL NPs into IC5-MOSECs. Conversely, ip. injection of FA-HDL(DiR-BOA) resulted in markedly improved targeting of the IC5-MOSEC cancer cells. The high expression of FR-α in IC5-MOSECs allows these cancer cells to readily take up FA conjugates. Thus by rerouting the HDL NPs to the FR-α, IC5-MOSECs are able to avidly internalize the FA-HDL NPs. Moreover, the local–regional delivery of FA-HDL(DiR-BOA) into the ip. cavity enables the IC5-MOSECs to extract these particles from their surroundings in a `first-pass' manner. This was demonstrated by the high levels of FA-HDL(DiR-BOA) detected both in the IC5-MOSEC tumors and ascites metastatic cells and the small amounts of this particle remaining in the cell-free fraction of the ascites fluid. The constituents of the ascites fluid include free-floating cancer cells and immune cells. While FA-HDL NP uptake is possible in both cell types (a subpopulation of monocytes are known to express a functional FR-α), the FR-α density on ovarian cancer cells (1–3 million/cell) is approximately 20-times greater than that on the immune cells [62]. This advantage in the expression of FR-α would favor the free-floating IC5-MOSECs to sequester much of the FA-HDL NPs in the peritoneal fluids. Furthermore, the IC5-MOSECs were also able to `outcompete' the normal host tissues for the FA-HDL NPs; significantly higher levels of the NPs were detected in the IC5-MOSECs than in any of the mouse organs. Fluorescence signal in the IC5-MOSEC tumors were three- to 14-times greater than that in the host liver. Drug/NP uptake into abdominal tissues following ip. administration primarily occurs through diffusion/convection across the tissue surface [63]. Once at the epithelial surface, the abundance of FR-α will dictate how avidly the particles are retained and internalized into tissues. For normal tissues, the distribution of FR-α is limited to just a few organs (kidneys, lung, chorid plexus and placenta) where the receptors are localized in the apical membranes facing their tubule lumen.[64,65] Thus ip. FA-HDL NPs would be unable to access the FR-α in these tissues. On the other hand, for the cancer cells the polarity of the FR-α is lost; [14,65] as such, this receptor is expressed at high levels all over the cell surface of the IC5-MOSECs fully exposed and accessible to the surrounding FA-HDL NPs in the peritoneal cavity. The pronounced selective uptake of FA-HDL NPs in the IC5-MOSEC tumors and metastatic ascites cells support this rationale. Additional independent studies have also shown that ip.-delivered anti-FR-α antibodies are able to selectively access ovarian cancer tumors and metastatic cells in the peritoneal cavity [66]. Under these conditions, the IC5-MOSEC tumors and metastatic cells experience much more favorable kinetics for pronounced FA-HDL NP uptake over the host tissues.

The emphasis of the current study focused on the selective targeting of the FA-HDL NPs towards ovarian cancer cells, and the next logical step would be to evaluate the therapeutic efficiency of this system to treat ovarian cancer. The core shell structure of the HDL NP makes it ideally suited to transport drugs with low water solubility. Interestingly, most chemotherapeutics tend to have poor water solubility [67]. The hydrophobic core of HDL typically ferries 100 molecules of cholesterol esters and triglycerides [68]. Exogenous lipophilic molecules can be substituted into the HDL core; however, their loading efficiency will be dependent upon their octanol:water partition properties. In this study, only four molecules of DiR-BOA were incorporated into HDL; however, this was an underestimation due to the presence of cholestryl oleate in the core. Several other studies have demonstrated

that various therapeutics (antiviral, antifungal and anticancer) can be successfully loaded into the HDL NP [33,69–73]. In these papers, each HDL molecule was reported to be able to carry between 25 and 40 molecules of drug. Moreover, the drug–HDL NP complex was shown to be stable for extended periods of time. Studies from the laboratory of Lacko are worth noting as they showed that the HDL NP was able to successfully transport paclitaxel (leading drug against ovarian cancer) and various siRNA species to cancer cells [33,72]. Regardless of which drug was investigated in these studies, each drug–HDL NP complex was shown to be therapeutically equal or more effective than the free drug [33,69–73]. Given that the present study clearly demonstrated that FR-α targeting was more effective than SR-BI targeting, it is anticipated that local–regional FA-HDL NP drug therapy will be highly efficacious against ovarian cancer. These studies are currently underway in our laboratory.

Conclusion

In summary, our findings demonstrate that the combination of ip. administration and active FR-α targeting significantly improved the delivery efficiency of FA-HDL NPs to tumor cells in a murine model of ovarian cancer. The deposition of nanoparicles in the ovarian cancer cells greatly exceeded that found in any of the host organs. Application of this general strategy (local–regional treatment coupled with active receptor targeting) can be extended to other preclinical and clinical settings to significantly improve the delivery efficiency of NP systems for cancer treatment or detection.

Future perspective

To date, there are many synthetic NPs actively being investigated for the purpose of anticancer drug delivery. Few of these candidates will ever make it to the clinic due to potential health and toxicity concerns surrounding the NP manufacturing processes, as well as the final NP materials. With the synthetic approaches, investigators not only have to overcome biological and kinetic challenges of tumor targeting, but they must also contend with the possible toxicological hazards of the carrier itself. Unlike the former products, the lipoprotein-based NPs are derived from endogenous plasma lipoproteins, and thus these carriers are fully biocompatible, biodegradable and nonimmunogenic. The natural proclivity of malignant cells to take up lipoprotein NPs makes these nanostructures even more attractive for anticancer drug delivery. However, before these natural carriers can be utilized in a clinical setting, concerns regarding the use of plasma products, batch-to-batch variability of lipoprotein isolations, and limited lipoprotein shelf life will all have to be addressed. Even more daunting are the biological and pharmacologic limitations posed by the high levels of circulating native lipoproteins and the pronounced uptake of lipoproteins by competing normal tissues (e.g., liver and adrenal glands). The findings of the present paper offer a strategy that overcomes these limitations. The combination of ligandconjugated lipoproteins and local–regional administration both increases the affinity of the NP for the intended tumor target and eliminates the competing uptake processes from normal tissues and the RES. Thus local–regional administration of ligand-conjugated lipoprotein NPs offers a plausible approach to markedly improve anticancer treatment, by enabling more specific drug targeting, and producing higher therapeutic potency and lower systemic toxicity.

Supplementary Material

Refer to Web version on PubMed Central for supplementary material.

Acknowledgments

The authors would like to thank H Li for expert technical assistance in this study. They would also like to thank M Krieger for the ldlA (mSR-BI) and ldlA7 cells and K Roby for the IC5-mouse ovarian surface epithelial cells.

This work was supported by the Canadian Institute of Health Research Grant 166453, J and T Tanenbaum/Brazilian Ball Chair in Prostate Cancer Research, University Health Network (G Zheng), and the University of Texas Southwestern – Small Animal Imaging Resource Program (IR Corbin; U24 CA126608).

No writing assistance was utilized in the production of this manuscript.

Ethical conduct of research The authors state that they have obtained appropriate institutional review board approval or have followed the principles outlined in the Declaration of Helsinki for all human or animal experimental investigations. In addition, for investigations involving human subjects, informed consent has been obtained from the participants involved.

References

Papers of special note have been highlighted as:

■ of interest

1. Parkin DM, Bray F, Ferlay J, Pisani P. Global cancer statistics, 2002. CA Cancer J. Clin. 2005; 55(2):74–108. [PubMed: 15761078]
2. Jemal A, Siegel R, Ward E, et al. Cancer statistics, 2008. CA Cancer J. Clin. 2008; 58(2):71–96. [PubMed: 18287387]
3. Scarberry KE, Dickerson EB, Zhang ZJ, Benigno BB, Mcdonald JF. Selective removal of ovarian cancer cells from human ascites fluid using magnetic nanoparticles. Nanomedicine. 2010; 6(3):399–408. [PubMed: 19969103]
4. Agarwal R, Kaye SB. Ovarian cancer: strategies for overcoming resistance to chemotherapy. Nat. Rev. Cancer. 2003; 3(7):502–516. [PubMed: 12835670]
5. Balvert-Locht HR, Coebergh JW, Hop WC, et al. Improved prognosis of ovarian cancer in The Netherlands during the period 1975–1985: a registry-based study. Gynecol. Oncol. 1991; 42(1):3–8. [PubMed: 1916506]
6. Ozols RF, Bundy BN, Greer BE, et al. Phase III trial of carboplatin and paclitaxel compared with cisplatin and paclitaxel in patients with optimally resected stage III ovarian cancer: a Gynecologic Oncology Group study. J. Clin. Oncol. 2003; 21(17):3194–3200. [PubMed: 12860964]
7. Markman M. Intraperitoneal chemotherapy is appropriate first line therapy for patients with optimally debulked ovarian cancer. Crit. Rev. Oncol. Hematol. 2001; 38(3):171–175. [PubMed: 11369252]
8. Howell SB, Pfeifle CE, Olshen RA. Intraperitoneal chemotherapy with melphalan. Ann. Intern. Med. 1984; 101(1):14–18. [PubMed: 6732077]
9. Zimm S, Cleary SM, Lucas WE, et al. Phase I/pharmacokinetic study of intraperitoneal cisplatin and etoposide. Cancer Res. 1987; 47(6):1712–1716. [PubMed: 3815369]
10. Morgan RR, Doroshow JH, Synold T, et al. Phase I trial of intraperitoneal docetaxel in the treatment of advanced malignancies primarily confined to the peritoneal cavity. Clin. Cancer Res. 2003; 9(16 Pt 1):5896–5901. [PubMed: 14676112]
11. Markman M, Rowinsky E, Hakes T, et al. Phase I trial of intraperitoneal taxol: a Gynecoloic Oncology Group study. J. Clin. Oncol. 1992; 10(9):1485–1491. [PubMed: 1355523]
12. Armstrong DK, Bundy B, Wenzel L, et al. Intraperitoneal cisplatin and paclitaxel in ovarian cancer. N. Engl. J. Med. 2006; 354(1):34–43. [PubMed: 16394300]
13. Anderson NJ, Hacker ED. Fatigue in women receiving intraperitoneal chemotherapy for ovarian cancer: a review of contributing factors. Clin. J. Oncol. Nurs. 2008; 12(3):445–454. [PubMed: 18515243]

14. Kalli KR, Oberg AL, Keeney GL, et al. Folate receptor alpha as a tumor target in epithelial ovarian cancer. Gynecol. Oncol. 2008; 108(3):619–626. [PubMed: 18222534] ■ Thorough examination of folate receptor-α expression in epithelial ovarian cancer.
15. Weitman SD, Lark RH, Coney LR, Al E. Distribution of folate recptor GP38 in normal and malignant cell lines and tissues. Cancer Res. 1992; 52:396–401.
16. Low PS, Henne WA, Doorneweerd DD. Discovery and development of folic-acid-based receptor targeting for imaging and therapy of cancer and inflammatory diseases. Acc. Chem. Res. 2008; 41(1):120–129. [PubMed: 17655275]
17. Leamon CP, Low PS. Delivery of macromolecules into living cells: a method that exploits folate receptor endocytosis. Proc. Natl Acad. Sci. USA. 1991; 88(13):5572–5576. [PubMed: 2062838]
18. Leamon CP, Low PS. Membrane folate-binding proteins are responsible for folate–protein conjugate endocytosis into cultured cells. Biochem. J. 1993; 291(Pt 3):855–860. [PubMed: 8387781]
19. Reddy JA, Xu LC, Parker N, Vetzel M, Leamon CP. Preclinical evaluation of (99m) Tc-EC20 for imaging folate receptor-positive tumors. J. Nucl. Med. 2004; 45(5):857–866. [PubMed: 15136637]
20. Kennedy MD, Jallad KN, Thompson DH, Ben-Amotz D, Low PS. Optical imaging of metastatic tumors using a folate-targeted fluorescent probe. J. Biomed. Opt. 2003; 8(4):636–641. [PubMed: 14563201]
21. Cheng Z, Thorek DL, Tsourkas A. Gadolinium-conjugated dendrimer nanoclusters as a tumor-targeted T1 magnetic resonance imaging contrast agent. Angew Chem. Int. Ed. Engl. 2010; 49(2): 346–350. [PubMed: 19967688]
22. Van Dam GM, Themelis G, Crane LM, et al. Intraoperative tumor-specific fluorescence imaging in ovarian cancer by folate receptor-alpha targeting: first in-human results. Nat. Med. 2011; 17(10): 1315–1319. [PubMed: 21926976] ■ Showcases the potential of folate receptor-targeted fluorescent probes to image tumors intraoperatively in human ovarian cancer.
23. Siegel BA, Dehdashti F, Mutch DG, et al. Evaluation of ^{111}In-DTPA-folate as a receptor-targeted diagnostic agent for ovarian cancer: initial clinical results. J. Nucl. Med. 2003; 44(5):700–707. [PubMed: 12732670]
24. Symanowski JT, Maurer AH, Naumann RW, Shah NP, Morgenstern D, Messmann RA. Use of ^{99m}Tc-EC20 (a folate-targeted imaging agent) to predict response to therapy with EC145 (folate-targeted therapy) in advanced ovarian cancer. ASCO Meeting Abstracts. 2010; 28(15 Suppl.): 5034.
25. Cao W, Ng KK, Corbin I, et al. Synthesis and evaluation of a stable bacteriochlorophyll-analog and its incorporation into high-density lipoprotein nanoparticles for tumor imaging. Bioconjug. Chem. 2009; 20(11):2023–2031. [PubMed: 19839633]
26. Chen W, Jarzyna PA, van Tilborg GAF, et al. RGD peptide functionalized and reconstituted high-density lipoprotein nanoparticles as a versatile and multimodal tumor targeting molecular imaging probe. FASEB J. 2010; 24(6):1689–1699. [PubMed: 20075195]
27. Corbin IR, Chen J, Cao W, Li H, Lund-Katz S, Zheng G. Enhanced cancer-targeted delivery using engineered high-density lipoprotein-based nanocarriers. JBN. 2007; 3(4):367–376.
28. Havel RJ, Eder HA, Bragdon JH. The distribution and chemical composition of ultracentrifugally separated lipoproteins in human serum. J. Clin. Invest. 1955; 34(9):1345–1353. [PubMed: 13252080]
29. Scanu A. Forms of human serum high density lipoprotein protein. J. Lipid Res. 1966; 7(2):295–306. [PubMed: 4957797]
30. Pittman RC, Glass CK, Atkinson D, Small DM. Synthetic high density lipoprotein particles. Application to studies of the apoprotein specificity for selective uptake of cholesterol esters. J. Biol. Chem. 1987; 262(6):2435–2442. [PubMed: 3029080] ■ Seminal study describing the preparation of high-density lipoprotein particles.
31. Zheng G, Chen J, Li H, Glickson JD. Rerouting lipoprotein nanoparticles to selected alternate receptors for the targeted delivery of cancer diagnostic and therapeutic agents. Proc. Natl Acad. Sci. USA. 2005; 102(49):17757–17762. [PubMed: 16306263] ■ First to describe the rerouting of lipoproteins to alternate receptors for the purposes of cancer detection and treatment.

32. Silva RA, Huang R, Morris J, et al. Structure of apolipoprotein A-I in spherical high density lipoproteins of different sizes. Proc. Natl Acad. Sci. 2008; 105(34):12176–12181. [PubMed: 18719128]
33. Shahzad MM, Mangala LS, Han HD, et al. Targeted delivery of small interfering RNA using reconstituted high-density lipoprotein nanoparticles. Neoplasia. 2011; 13(4):309–319. [PubMed: 21472135]
34. Skajaa T, Cormode DP, Jarzyna PA, et al. The biological properties of iron oxide core high-density lipoprotein in experimental atherosclerosis. Biomaterials. 2011; 32(1):206–213. [PubMed: 20926130]
35. Murakami T, Wijagkanalan W, Hashida M, Tsuchida K. Intracellular drug delivery by genetically engineered high-density lipoprotein nanoparticles. Nanomedicine (Lond.). 2010; 5(6):867–879. [PubMed: 20735223]
36. Zhou P, Hatziieremia S, Elliott Ma, et al. Uptake of synthetic low density lipoprotein by leukemic stem cells – a potential stem cell targeted drug delivery strategy. J. Control. Release. 2010; 148(3): 380–387. [PubMed: 20869412]
37. Marotta DE, Cao WG, Wileyto EP, et al. Evaluation of bacteriochlorophyll-reconstituted low-density lipoprotein nanoparticles for photodynamic therapy efficacy *in vivo*. Nanomedicine. 2011; 6(3):475–487. [PubMed: 21542686]
38. Hill ML, Corbin IR, Levitin RB, et al. *In vitro* assessment of poly-iodinated triglyceride reconstituted low-density lipoprotein: initial steps toward CT molecular imaging. Acad. Radiol. 2010; 17(11):1359–1365. [PubMed: 20719547]
39. Ng KK, Lovell JF, Zheng G. Lipoprotein-inspired nanoparticles for cancer theranostics. Acc. Chem. Res. 2011; 44(10):1105–1113. [PubMed: 21557543]
40. Rensen PC, De Vrueh RL, Kuiper J, Bijsterbosch MK, Biessen EA, Van Berkel TJ. Recombinant lipoproteins: lipoprotein-like lipid particles for drug targeting. Adv. Drug Deliv. Rev. 2001; 47(2–3):251–276. [PubMed: 11311995]
41. Mahley RW, Innerarity TL, Rall SC Jr, Weisgraber KH. Plasma lipoproteins: apolipoprotein structure and function. J. Lipid Res. 1984; 25(12):1277–1294. [PubMed: 6099394]
42. Thuahnai ST, Lund-Katz S, Anantharamaiah GM, Williams DL, Phillips MC. A quantitative analysis of apolipoprotein binding to SR-BI: multiple binding sites for lipid-free and lipid-associated apolipoproteins. J. Lipid Res. 2003; 44(6):1132–1142. [PubMed: 12671027]
43. Kader A, Pater A. Loading anticancer drugs into HDL as well as LDL has little affect on properties of complexes and enhances cytotoxicity to human carcinoma cells. J. Control. Release. 2002; 80(1–3):29–44. [PubMed: 11943385]
44. Corbin, IR.; Ng, K.; Zheng, G. Lipoprotein-based nanoplatforms for cancer molecular imaging. In: Chen, X., editor. Nanoplatform-Based Molecular Imaging. John Wiley & Sons; NJ, USA: 2011. p. 431-462.
45. Chen J, Corbin IR, Li H, Cao W, Glickson JD, Zheng G. Ligand conjugated low-density lipoprotein nanoparticles for enhanced optical cancer imaging *in vivo*. J. Am. Chem. Soc. 2007; 129(18):5798–5799. [PubMed: 17428054]
46. Weitman SD, Lark RH, Coney LR, et al. Distribution of the folate receptor GP38 in normal and malignant cell lines and tissues. Cancer Res. 1992; 52(12):3396–3401. [PubMed: 1596899]
47. Parker N, Turk MJ, Westrick E, Lewis JD, Low PS, Leamon CP. Folate receptor expression in carcinomas and normal tissues determined by a quantitative radioligand binding assay. Anal. Biochem. 2005; 338(2):284–293. [PubMed: 15745749]
48. Krieger M. Charting the fate of the `good cholesterol': identification and characterization of the high-density lipoprotein receptor SR-BI. Annu. Rev. Biochem. 1999; 68:523–558. [PubMed: 10872459]
49. Acton S, Rigotti A, Landschulz KT, Xu S, Hobbs HH, Krieger M. Identification of scavenger receptor SR-BI as a high density lipoprotein receptor. Science. 1996; 271(5248):518–520. [PubMed: 8560269]
50. Werner ME, Karve S, Sukumar R, et al. Folate-targeted nanoparticle delivery of chemo- and radiotherapeutics for the treatment of ovarian cancer peritoneal metastasis. Biomaterials. 2011; 32(33):8548–8554. [PubMed: 21843904]

51. Roby KF, Taylor CC, Sweetwood JP, et al. Development of a syngeneic mouse model for events related to ovarian cancer. Carcinogenesis. 2000; 21(4):585–591. [PubMed: 10753190] ■ A practical and representative mouse model of ovarian cancer is described.
52. Litterst CL, Collins JM, Lowe MC, Arnold ST, Powell DM, Guarino AM. Local and systemic toxicity resulting from large-volume ip. administration of doxorubicin in the rat. Cancer Treat. Rep. 1982; 66(1):157–161. [PubMed: 7053251]
53. Markman M, George M, Hakes T, et al. Phase II trial of intraperitoneal mitoxantrone in the management of refractory ovarian cancer. J. Clin. Oncol. 1990; 8(1):146–150. [PubMed: 2295905]
54. Bajaj G, Yeo Y. Drug delivery systems for intraperitoneal therapy. Pharm. Res. 2010; 27(5):735–738. [PubMed: 20198409]
55. Cho YW, Park SA, Han TH, et al. *In vivo* tumor targeting and radionuclide imaging with self-assembled nanoparticles: mechanisms, key factors, and their implications. Biomaterials. 2007; 28(6):1236–1247. [PubMed: 17126900]
56. Choi CH, Alabi CA, Webster P, Davis ME. Mechanism of active targeting in solid tumors with transferrin-containing gold nanoparticles. Proc. Natl Acad. Sci. USA. 2010; 107(3):1235–1240. [PubMed: 20080552]
57. Kukowska-Latallo JF, Candido KA, Cao Z, et al. Nanoparticle targeting of anticancer drug improves therapeutic response in animal model of human epithelial cancer. Cancer Res. 2005; 65(12):5317–5324. [PubMed: 15958579]
58. Zhao R, Diop-Bove N, Visentin M, Goldman ID. Mechanisms of membrane transport of folates into cells and across epithelia. Annu. Rev. Nutr. 2011; 31:177–201. [PubMed: 21568705]
59. Wang Y, Zhao R, Russell RG, Goldman ID. Localization of the murine reduced folate carrier as assessed by immunohistochemical analysis. Biochem. Biophys. Acta. 2001; 1513(1):49–54. [PubMed: 11427193]
60. Qiu A, Jansen M, Sakaris A, et al. Identification of an intestinal folate transporter and the molecular basis for hereditary folate malabsorption. Cell. 2006; 127(5):917–928. [PubMed: 17129779]
61. Yeo Y, Xu P. Nanoparticles for tumor-specific intracellular drug delivery. Conf. Proc. IEEE Eng. Med. Biol. Soc. 2009:2403–2405. [PubMed: 19964955]
62. He W, Kularatne SA, Kalli KR, et al. Quantitation of circulating tumor cells in blood samples from ovarian and prostate cancer patients using tumor-specific fluorescent ligands. Int. J. Cancer. 2008; 123(8):1968–1973. [PubMed: 18661519]
63. Dedrick, Rl; Flessner, MF. Pharmacokinetic problems in peritoneal drug administration: tissue penetration and surface exposure. J. Natl Cancer Inst. 1997; 89(7):480–487. [PubMed: 9086004]
64. Weitman SD, Weinberg AG, Coney LR, Zurawski VR, Jennings DS, Kamen BA. Cellular localization of the folate receptor: potential role in drug toxicity and folate homeostasis. Cancer Res. 1992; 52(23):6708–6711. [PubMed: 1330299]
65. Patrick TA, Kranz DM, van Dyke TA, Roy EJ. Folate receptors as potential therapeutic targets in choroid plexus tumors of SV40 transgenic mice. J. Neuro-Oncol. 1997; 32(2):111–123.
66. Zacchetti A, Martin F, Luison E, et al. Antitumor effects of a human dimeric antibody fragment 131I-AFRA-DFM5.3 in a mouse model for ovarian cancer. J. Nucl. Med. 2011; 52(12):1938–1946. [PubMed: 22068897]
67. JB Lippincott Company. Cancer Chemotherapy: Principles and Practice. Chabner, BA.; Collins, JM., editors. JB Lippincott Company; PA, USA: 1990.
68. Shen BW, Scanu AM, Kezdy FJ. Structure of human serum lipoproteins inferred from compositional analysis. Proc. Natl Acad. Sci. USA. 1977; 74(3):837–841. [PubMed: 265578]
69. Bijsterbosch MK, Schouten D, Van Berkel TJ. Synthesis of the dioleoyl derivative of iododeoxyuridine and its incorporation into reconstituted high density lipoprotein particles. Biochemistry. 1994; 33(47):14073–14080. [PubMed: 7947817]
70. Lou B, Liao XL, Wu MP, Cheng PF, Yin CY, Fei Z. High-density lipoprotein as a potential carrier for delivery of a lipophilic antitumoral drug into hepatoma cells. World J. Gastroenterol. 2005; 11(7):954–959. [PubMed: 15742395]

71. Oda MN, Hargreaves PL, Beckstead JA, Redmond KA, Van Antwerpen R, Ryan RO. Reconstituted high density lipoprotein enriched with the polyene antibiotic amphotericin B. J. Lipid Res. 2006; 47(2):260–267. [PubMed: 16314670]

72. Mcconathy WJ, Nair MP, Paranjape S, Mooberry L, Lacko AG. Evaluation of synthetic/reconstituted high-density lipoproteins as delivery vehicles for paclitaxel. Anticancer Drugs. 2008; 19(2):183–188. [PubMed: 18176115] ■ Formulation of high-density lipoprotein particles with paclitaxel.

73. Sabnis N, Nair M, Israel M, Mcconathy WJ, Lacko AG. Enhanced solubility and functionality of valrubicin (AD-32) against cancer cells upon encapsulation into biocompatible nanoparticles. Int. J. Nanomedicine. 2012; 7:975–983. [PubMed: 22393294]

Executive summary

Functionalizing high-density lipoprotein nanoparticles to target ovarian cancer

- Over 90% of epithelial ovarian cancers overexpress the high-affinity folate receptor-α (FR-α).
- Engineered high-density lipoprotein (HDL) nanoparticles (NPs) are fully biocompatible, naturally able to evade reticular endothelium system surveillance and possess long circulation kinetics.
- Conjugating folic acid (FA) to HDL NPs simultaneously abolishes this carrier's affinity for the scavenger receptor class B type I (HDL receptor) and reroutes its targeting to the FR-α.

FA-HDL NPs have a high affinity for ovarian cancer cells

- The IC5 mouse ovarian surface epithelial cells (IC5-MOSEC) murine model of ovarian cancer closely reproduces the pathology seen in the human malignancy.
- FA-HDL NPs bind more avidly to and are internalized in IC5-MOSEC ovarian cancer cells more than HDL NPs.
- The FR-α mediates uptake of FA-HDL NPs in IC5-MOSEC ovarian cancer cells.

In vivo **evidence of enhanced FA-HDL NP targeting to ovarian cancer**

- Intravenous administration of FA-HDL into mice with IC5-MOSEC-induced metastatic ovarian cancer resulted in the majority of the NPs being deposited in the liver.
- Intraperitoneal (ip.) injection of HDL NPs into ovarian cancer-bearing mice had a broad distribution of the NPs across the host tissues and tumor cells.
- Ip. injection of FA-HDL NPs into ovarian cancer-bearing mice resulted in high uptake of the NP in IC5-MOSEC tumor cells and minimal amounts in host liver.
- The combination of local–regional ip. administration and active FR-α targeting provides an efficacious means of selective drug delivery to ovarian cancer cells.

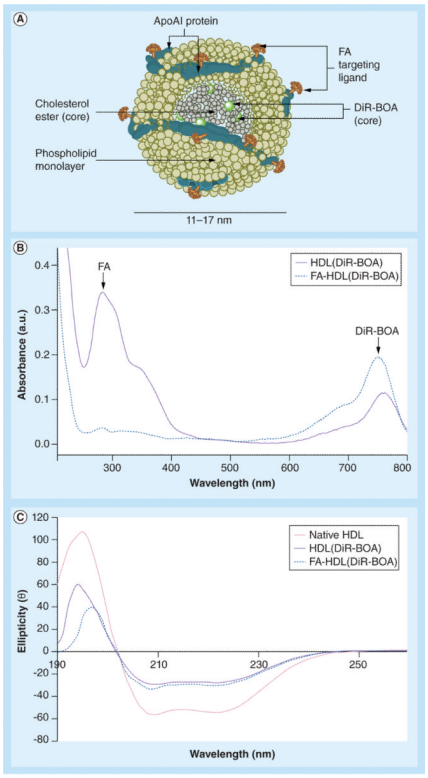

Figure 1. Structural scheme and spectrometric properties of folic acid-conjugated high density lipoprotein(DiR-BOA)

(A) Schematic structure of FA-HDL(DiR-BOA). **(B)** UV spectra of HDL(DiR-BOA) and FA-HDL(DiR-BOA). Characteristic peaks belonging to DiR(BOA) and FA are identified at 750 nm and 285 nm, respectively. **(C)** Circular dichroism spectra of native HDL, HDL(DiR-BOA) and of FA-HDL(DiR-BOA). The α-helix secondary structure of apoAI is monitored by changes in ellipticity at 222 nm. DiR-BOA: 1,1′-dioctadecyl-3,3,3′,3′-tetramethylindo tricarbocyanine iodide bis-oleate; FA: Folic acid; HDL: High-density lipoprotein.

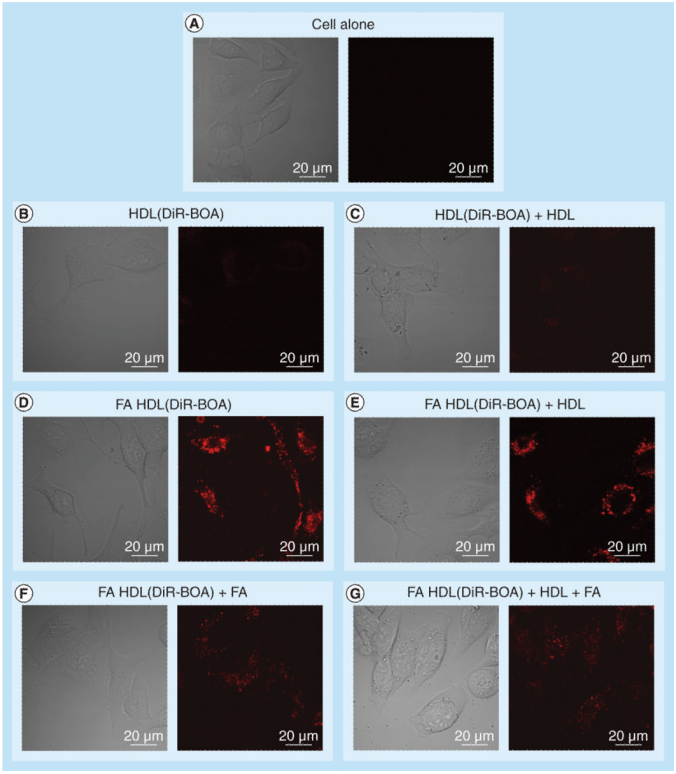

Figure 2. Fluorescent and corresponding bright-field confocal images of IC5 mouse ovarian surface epithelial cells incubated with high-density lipoprotein(DiR-BOA) (1.6 μM) or folic acid-conjugated high-density lipoprotein(DiR-BOA) (1.6 μM) for 3 h (high voltage = 700)

The inhibition studies were performed with 20-fold excess native HDL and 600-fold excess of FA. DiR-BOA: 1,1′-dioctadecyl-3,3,3′,3′-tetramethylindo tricarbocyanine iodide bis-oleate; FA: Folic acid; HDL: High-density lipoprotein.

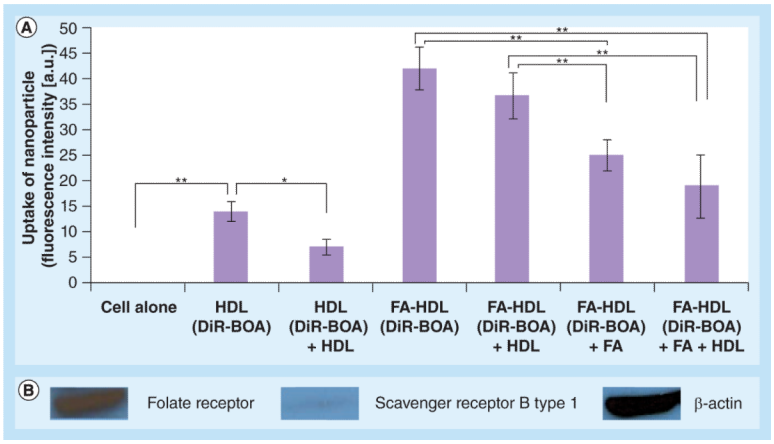

Figure 3. Flow cytometry studies of IC5 mouse ovarian surface epithelial cells following a 3-h incubation with high-density lipoprotein(DiR-BOA) (1.6 μM) or folic acid-conjugated high-density lipoprotein(DiR-BOA) (1.6 μM) for 3 h

(A) The inhibition studies were performed with 20-fold excess native HDL and 600-fold excess of FA. Values represent mean ± standard deviation. **(B)** Western blot of folate receptor, scavenger receptor B type 1 and corresponding β-actin protein expression in IC5 mouse ovarian surface epithelial cells.

*Represents a significant difference ($p < 0.05$).

**Represents a significant difference ($p < 0.0001$).

DiR-BOA: 1,1′-dioctadecyl-3,3,3′,3′-tetramethylindo tricarbocyanine iodide bis-oleate; FA: Folic acid; HDL: High-density lipoprotein.

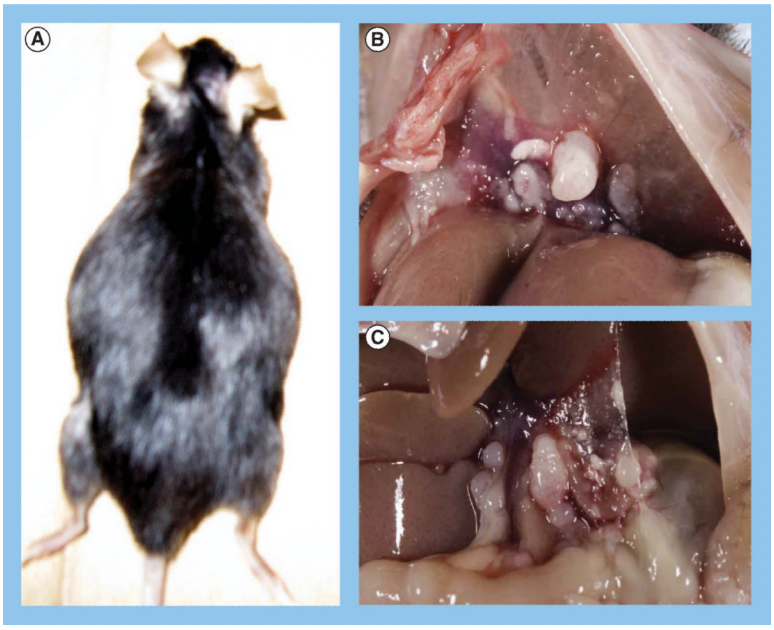

Figure 4. IC5 mouse ovarian surface epithelial cell mouse model of metastatic ovarian cancer

(A) Dorsal view of female mouse with advanced metastatic ovarian cancer induced by intraperitoneal injection of IC5 mouse ovarian surface epithelial cells. The distended abdomen is indicative of accumulation of ascites. Metastatic tumor foci on **(B)** diaphragm and **(C)** mesenteries.

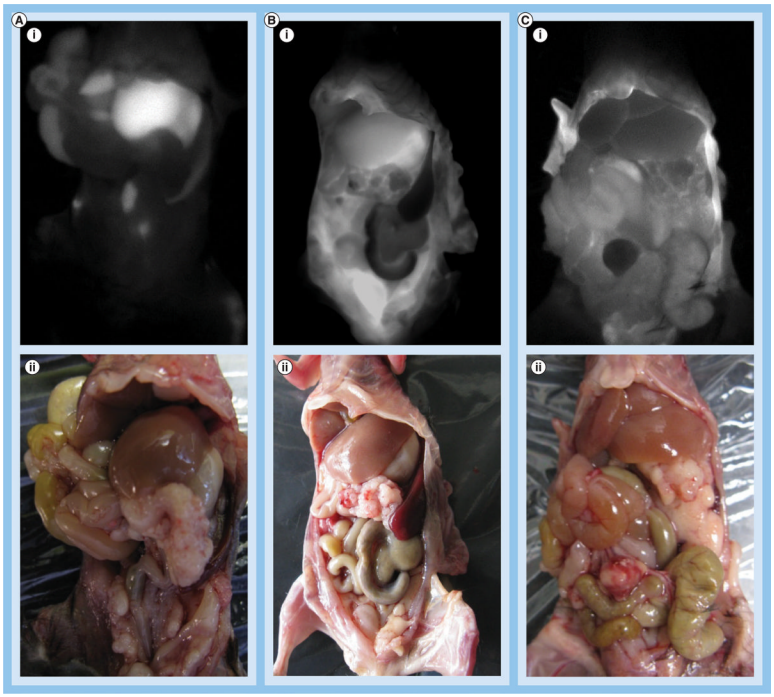

Figure 5. ***In vivo*** **fluorescence imaging of tumor-bearing mice following different routes of high-density lipoprotein (DiR-BOA) or folic acid-conjugated high-density lipoprotein(DiR-BOA) administration**

In vivo **(i)** fluorescent and **(ii)** light images of tumor-bearing female mice 24 h following: **(A)** intravenous injection of folic acid-conjugated high-density lipoprotein (FA-HDL[DiR-BOA]) (4 nmol); **(B)** intraperitoneal injection of HDL(DiR-BOA) (4 nmol); or **(C)** intraperitoneal injection of FA-HDL(DiR-BOA) (4 nmol).
DiR-BOA: 1,1′-dioctadecyl-3,3,3′,3′-tetramethylindo tricarbocyanine iodide bis-oleate.

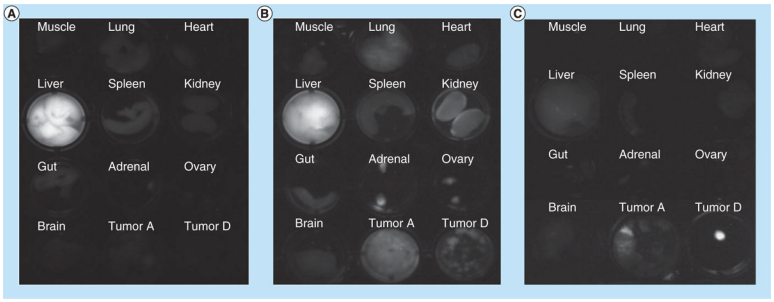

Figure 6. ***Ex vivo*** **fluorescence imaging of mouse tissues and tumors following different routes of high-density lipoprotein (DiR-BOA) or folic acid-conjugated high-density lipoprotein(DiR-BOA) administration**

Fluorescent image of excised organs and tumor 24 h after: **(A)** intravenous injection of folic acid-conjugated high-density lipoprotein (FA-HDL)(DiR-BOA) (4 nmol); **(B)** intraperitoneal injection of HDL(DiR-BOA) (4 nmol); or **(C)** intraperitoneal injection of FA-HDL(DiR-BOA) (4 nmol). Tumor A indicates metastatic tumors collected from the abdominal cavity. Tumor D indicates metastatic tumors collected from the diaphragm. DiR-BOA: 1,1′-dioctadecyl-3,3,3′,3′-tetramethylindo tricarbocyanine iodide bis-oleate.

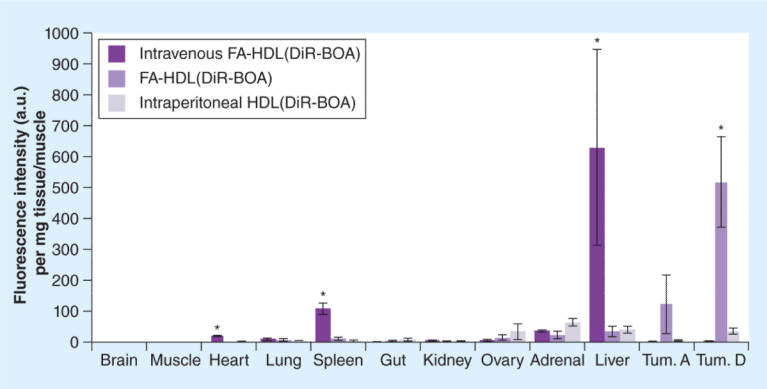

Figure 7. Biodistribution of intravenous folic acid-conjugated high-density lipoprotein(DiR-BOA), intraperitoneal high-density lipoprotein(DiR-BOA) and folic acid-conjugated high-density lipoprotein(DiR-BOA) in tumor-bearing mice 24 h after respective nanoparticle administration

Data units are DiR-BOA fluorescence intensity per mg of tissue all normalized to muscle tissue values. Data reflects mean ± standard deviation (n = 3–4 mice per group). Tum. A indicates metastatic tumors collected from abdominal cavity. Tum. D indicates metastatic tumors collected from the diaphragm.

*Represents a significant difference from corresponding groups ($p < 0.05$).

DiR-BOA: 1,1′-dioctadecyl-3,3,3′,3′-tetramethylindo tricarbocyanine iodide bis-oleate; FA: Folic acid; HDL: High-density lipoprotein; Tum.: Tumor.

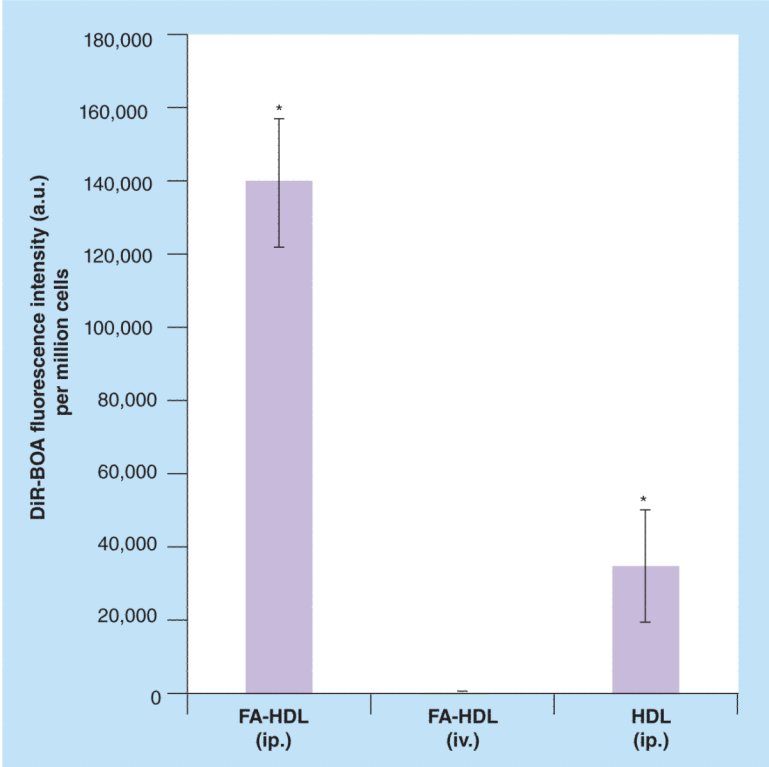

Figure 8. Uptake of folic acid-conjugated high-density lipoprotein(DiR-BOA) or high-density lipoprotein(DiR-BOA) in ascites cells 24 h following intravenous or intraperitoneal injections

Data units are DiR-BOA fluorescence intensity per million cells. Data reflects mean ± standard deviation (n = 3–4 mice per group).

*Represents a significance difference from other groups ($p < 0.05$).

DiR-BOA: 1,1′-dioctadecyl-3,3,3′,3′-tetramethylindo tricarbocyanine iodide bis-oleate; FA: Folic acid; HDL: High-density lipoprotein; ip.: Intraperitoneal; iv.: Intravenous.

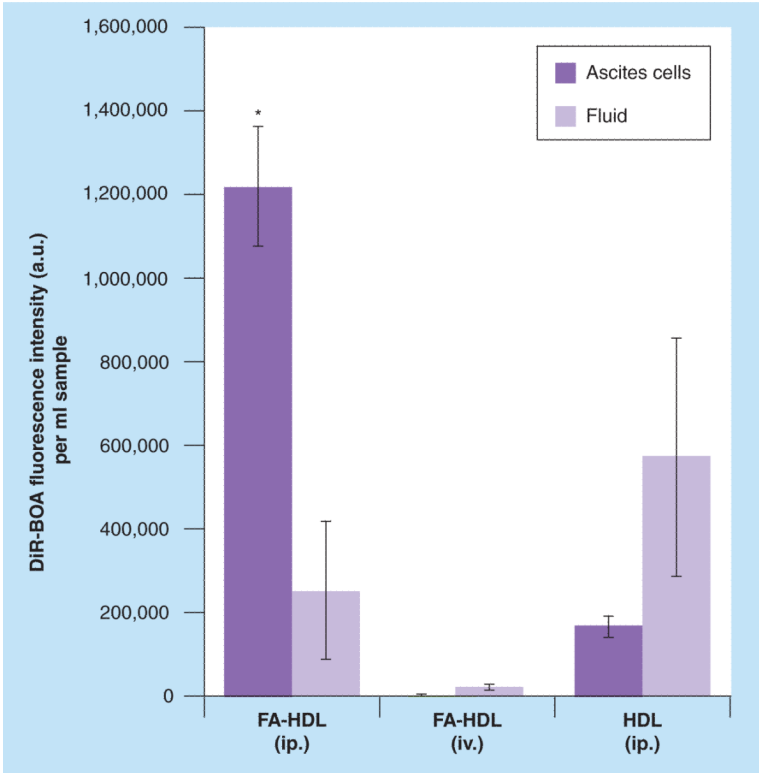

Figure 9. Comparison of folic acid-conjugated high-density lipoprotein(DiR-BOA) or high-density lipoprotein(DiR-BOA) concentrations in ascites cells or fluid 24 h following intravenous or intraperitoneal injections

Data units are DiR-BOA fluorescence intensity per ml of sample. Data reflects mean ± standard deviation (n = 3 mice per group).

*Represents a significance difference from corresponding groups ($p < 0.05$).

FA: Folic acid; HDL: High-density lipoprotein; ip.: Intraperitoneal; iv.: Intravenous.